Sensors and Materials, Vol. 34, No. 2 (2022) 603–610
MYU Tokyo

S & M 2832

Comparative Study of Optical and Scintillation Properties of Tm-doped $La_2Si_2O_7$ and $Lu_2Si_2O_7$ Single Crystals

Prom Kantuptim,* Daisuke Nakauchi, Takumi Kato,
Noriaki Kawaguchi, and Takayuki Yanagida

Division of Materials Science, Graduate School of Science and Technology,
Nara Institute of Science and Technology, 8916-5 Takayama, Ikoma, Nara 630-0192, Japan

(Received October 13, 2021; accepted November 30, 2021)

Keywords: lanthanum pyrosilicate, lutetium pyrosilicate, thulium, photoluminescence, pulse height

Lanthanum and lutetium pyrosilicate ($La_2Si_2O_7$ and $Lu_2Si_2O_7$, respectively) single crystals with a Tm doping concentration of 2.0% were successfully synthesized by the floating-zone method. X-ray diffraction patterns showed a single phase in each compound without the impurity phase. Both their photoluminescence (PL) and scintillation properties were systematically determined in this study, including PL emission, PL decay time, X-ray-induced scintillation spectra, X-ray-induced scintillation decay time, afterglow level, and pulse height spectra. The emission from Tm^{3+} 4f–4f transition was observed on both samples as shown by PL emission as well as X-ray-induced scintillation spectra. Under ^{137}Cs 662 keV γ-ray irradiation, their scintillation light yields were 2340 ph/MeV for Tm-doped $Lu_2Si_2O_7$ and 1440 ph/MeV for Tm-doped $La_2Si_2O_7$.

1. Introduction

At present, ionizing radiation is utilized in many aspects of our life. Improvements of the tools for ionizing radiation detection are necessary in both scientific and industrial sectors. A scintillator is a subcategory in luminescence materials that have the unique ability to convert ionizing radiations such as γ-ray, α-ray, and X-ray into low-energy photons such as UV, visible, or near-infrared light. With the combination of the scintillator and a suitable photodetector called the scintillation detector, ionizing radiation is detected. With this ability, the scintillation detector has been implemented for various professional purposes, including astrophysics,[1] medicine,[2] natural resource exploration,[3] homeland security,[4] and many more fields. For several decades until now, solid-state scintillators in various forms of materials, including plastics,[5] glasses,[6–10] single crystals,[11–16] transparent ceramics,[17–20] and composite materials, have been developed.[21,22] Among all the possible materials, single crystals are one of the promising choices because the single-crystal scintillator has many advantages, including high chemical stability, transparency, and high scintillation light yield. An obvious disadvantage is the typically higher cost to produce single crystals. In the early 2000s, the pyrosilicate single

*Corresponding author: e-mail: prom.kantuptim.pf2@ms.naist.jp
https://doi.org/10.18494/SAM3690

ISSN 0914-4935
https://myukk.org/

crystal with the lanthanide ion luminescence center for novel scintillators became an interesting research topic with the introduction of Ce-doped $Lu_2Si_2O_7$ (LPS) with the fast decay time of 38 ns and the impressive scintillation light yield of 26300 ph/MeV.[23] Our group also extensively studied the scintillation properties of pyrosilicate materials, including LPS, $Y_2Si_2O_7$ (YPS), and $Gd_2Si_2O_7$ (GPS), to investigate these compounds in more detail.[24,25]

Recently, a number of studies on Ce-doped $La_2Si_2O_7$ (LaPS) have shown interesting results on this newly investigated material in the pyrosilicate group, such as a low afterglow level of around 30–56 ppm and a respective light yield of 5400 ph/MeV.[26,27] Given these previous studies on LaPS, a comparative study between LaPS and other conventional pyrosilicate materials, especially LPS, is considered necessary. In addition, we studied the Tm doping concentration dependence of LPS[28] and selected the best concentration (2.0%) for the comparative study in this project. In this study, we aim to investigate the photoluminescence (PL) and scintillation properties of 2.0% Tm-doped LaPS and LPS, including PL emission, PL decay time, scintillation spectra, and scintillation decay time, and their detector perspective properties such as scintillation light yield as well as afterglow level.

2. Materials and Methods

The Tm-doped LaPS and LPS single crystals were prepared in the following order. First, high-purity raw material powders, including SiO_2 (99.99%), La_2O_3 (99.99%), Lu_2O_3 (99.99%), and Tm_2O_3 (99.99%), were weighed and mixed in an agate mortar and put in a flexible mold. The Tm concentration was 2.0 mol% with respect to La and Lu for LaPS and LPS, respectively. Hydrostatic pressure was applied to each mixed powder for rod shaping, and LaPS and LPS rods were sintered at 1400 °C for 10 h and 1250 °C for 8 h, respectively. The obtained ceramic rods were crystallized using a dual-halogen-type desktop floating zone furnace (Canon Machinery FZD0192) with a pulling down rate of 5 mm/h. The single-crystal rods were cut and polished on both surfaces for further optical evaluation. Some of the residual pieces of the crystal from the cutting process were ground using the agate mortar to a fine powder for X-ray diffraction (XRD) analysis with an X-ray diffractometer (Rigaku MiniFlex600).

The PL emission maps were measured using Quantaurus-QY (Hamamatsu Photonics C11347-01). The emission maps were observed in the excitation wavelength range of 300–380 nm and in the emission wavelength range of 400–900 nm. The PL quantum yield (QY) was calculated as $QY = N_e/N_a$, where N_e is the number of photons emitted as photoluminescence from the sample and N_a is the number of photons absorbed by the sample. The PL decay time profiles were measured using Quantaurus-τ (Hamamatsu Photonics C11367). The wavelength range of the excitation light was controlled using a 340–360 nm bandpass filter (Asahi spectra BP340-360) and a 470 nm long-pass filter (Asahi spectra SCF470) for the emission light.

For the scintillation properties, X-ray-induced scintillation spectroscopy, X-ray-induced scintillation decay time analysis, and afterglow analysis were carried out using our original instrument setups.[29,30] The observation wavelengths of scintillation decay time and afterglow were in the UV–visible range (160–650 nm). In addition, the afterglow level at 20 ms after X-ray irradiation (Af_{20}) was calculated as $Af_{20} = (I_{20} - I_{bg})/I_{max}$, where I_{20} is the signal intensity at 20 ms

after X-ray irradiation, I_{bg} is the signal intensity before X-ray irradiation (background), and I_{max} is the signal intensity during X-ray irradiation.

For the γ-ray-induced properties, the pulse height measurement was carried out using our original setup.[31] In this measurement, a photomultiplier (PMT) (Hamamatsu R7600-200) was used as a photodetector, the shaping time of a shaping amplifier (ORTEC 572) was adjusted to 10 μs, and ^{137}Cs was selected as the 662 keV γ-ray source. In the pulse-height analysis, the light yield under 662 keV γ-ray irradiation was calculated using a Ce-doped Gd_2SiO_5 (GSO) sample as reference with an absolute scintillation light yield of 7000 ph/MeV.

3. Results and Discussion

3.1 Sample condition

Figure 1(A) shows photographs of the Tm-doped LaPS and LPS single crystals synthesized by the floating-zone method with notable cracks throughout the crystal rods. The sizes of the as-grown single crystal rods were 4 mm ϕ × 22 mm for the Tm-doped LaPS sample and 4 mm ϕ × 15 mm for the Tm-doped LPS sample. On the other hand, Fig. 1(B) shows photographs of the cut and polished samples of Tm-doped LaPS and LPS single crystals. Results of the crystal growth experiments revealed that the LPS crystal is easier to grow than the LaPS crystal because the ionic radius of Tm^{3+} (87 pm) is more similar to that of Lu^{3+} (86 pm) than to that of La^{3+} (106 pm). A fraction of each crystal was ground for the powder XRD analysis, and Fig. 2 shows the XRD patterns of the Tm-doped LaPS and LPS samples, including the reference XRD patterns of $La_2Si_2O_7$ (JCPDS 82-0729) and $Lu_2Si_2O_7$ (COD 8100597). In the comparison between the samples and the references, impurity phases such as La_2SiO_5 from the La_2O_3–SiO_2 binary system as well as Lu_2SiO_5 or $Lu_4Si_3O_{12}$ from the phase diagram of the Lu_2O_3–SiO_2 binary system cannot be found in the XRD patterns of the Tm-doped LaPS and LPS samples.[32,33]

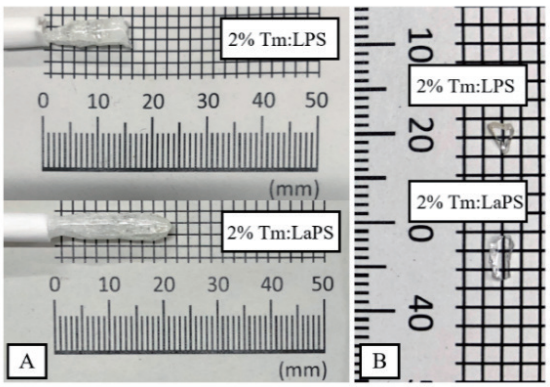

Fig. 1. (Color online) Photographs of (A) Tm-doped LaPS and LPS single crystals as-grown and (B) after cutting and polishing.

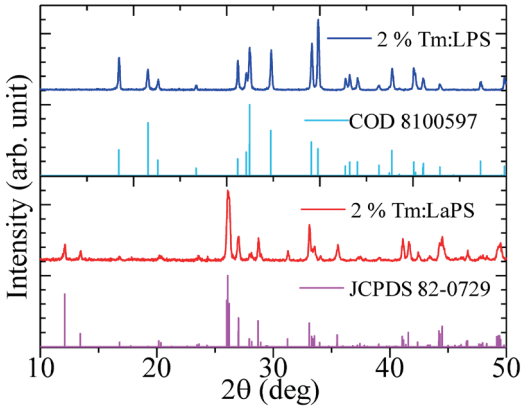

Fig. 2. (Color online) XRD patterns of Tm-doped LaPS and LPS samples.

3.2 Photoluminescence properties

Figure 3 shows the PL emission contour graphs of the Tm-doped LaPS and LPS samples. The PL emission maps of these samples were similar at around 450 nm emission. The emission band at 450 nm originated from the 4f–4f transition of Tm^{3+},[34] which was observed in both samples. However, the Tm-doped LaPS sample did not show any emission such as host emission, but low-concentration Tm-doped LPS samples showed host emission at around 800–900 nm in our previous study.[28] In addition, the Tm-doped LaPS sample showed PL *QY* at 5.0%. Similarly, the Tm-doped LPS sample also showed PL *QY* at 4.9%. In addition, the obtained PL *QY* values of these two samples were lower than those of the same host materials with other lanthanide dopants, such as Ce-doped LaPS (27.8%)[26] and Pr-doped LPS (22.6%).[25]

The PL decay time profiles of the Tm-doped LaPS and LPS samples are presented in Fig. 4. Excitation and observation wavelengths were selected by focusing on the Tm^{3+} 4f–4f emission from the previous result on PL emission. The PL decay time profiles of both samples were fitted with two exponential functions. The first decay time constant (τ_1) values were 1.0 and 2.0 μs for the Tm-doped LPS and LaPS samples, respectively. This decay component originated from the instrumental response function as shown by the green line in the figure.

The second decay time constant (τ_2) values were 81.6 and 118.6 μs for the Tm-doped LPS and LaPS samples, respectively. These decay time constants originated from the 4f–4f transition of Tm^{3+} and are similar to those of the Tm-doped $SrWO_4$ sample studied by Jia *et al.*[35] In addition, the τ_2 of the 2.0% Tm-doped LaPS sample is very similar to that of our 1.0% Tm-doped LPS sample from the last study at 113.4 μs.

3.3 Scintillation properties

Figure 5 shows X-ray-induced scintillation spectra of the Tm-doped LaPS and LPS samples with the undoped LaPS and LPS. In addition, the intensities shown in this figure only represent

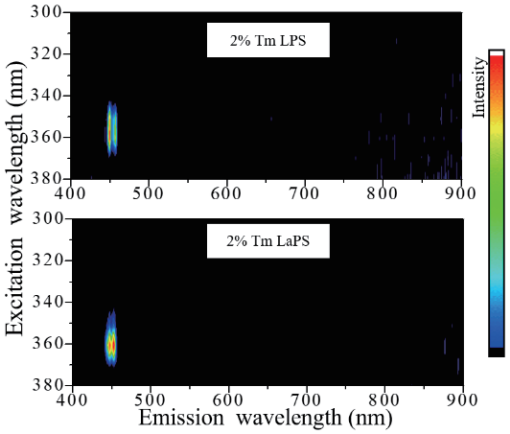

Fig. 3. (Color online) PL emission contour graphs of Tm-doped LaPS and LPS samples.

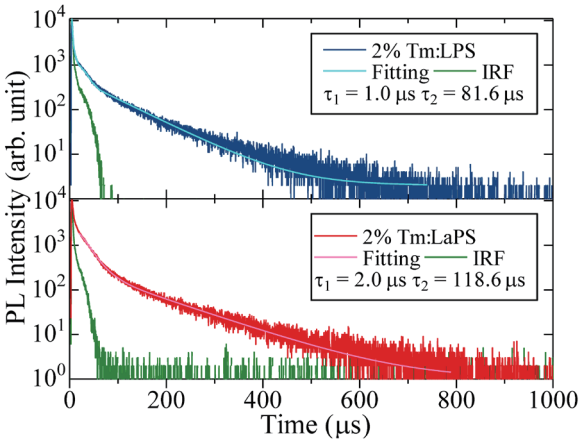

Fig. 4. (Color online) PL decay time profiles of Tm-doped LaPS and LPS samples.

the qualitative values, and the comparison with the scintillation light yield is discussed on the basis of the pulse-height spectra. Both samples have the same spectral shapes with different intensities of each emission peak. Both samples exhibited two high-intensity emission peaks at 360 nm from the $^1D_2 \rightarrow {}^3H_6$ transition and 460 nm from the $^1G_4 \rightarrow {}^3H_6$ transition.[36] In the 360 nm scintillation, both sample spectra at around 360 nm shifted minimally owing to the influence from the self-trapped exciton (STE) in the similar wavelength region, as indicated in the spectra of undoped LaPS and LPS.[24] In addition to those peaks, both samples exhibited a low-intensity emission at 290 nm from the $^1I_6 \rightarrow {}^3H_6$ transition of Tm^{3+}.[37]

Figure 6 shows the X-ray-induced scintillation decay time profiles of the Tm-doped LaPS and LPS samples. The scintillation decay time profiles of both samples were fitted by three exponential functions, and the decay constants are presented in the figure. The τ_1 values of 4.7 μs for the Tm-doped LPS and 3.3 μs for the Tm-doped LaPS originated from the 290 nm scintillation ($^1I_6 \rightarrow {}^3H_6$ transition), which appeared previously on the X-ray-induced scintillation spectra. The τ_2 values of 20.3 μs for the Tm-doped LPS sample and 17.4 μs for the Tm-doped LaPS sample originated from the 360 nm scintillation ($^1D_2 \rightarrow {}^3H_6$ transition). In addition, the first two components of both the Tm-doped LaPS and LPS samples are in a range similar to the Tm^{3+} 4f–4f decay time constant found in Tm-doped $Y_3Al_5O_{12}$ (YAG) and Tm-doped $Lu_3Al_5O_{12}$ (LuAG).[38] Finally, the τ_3 values of 74.4 μs for the Tm-doped LPS sample and 115.5 μs for the Tm-doped LaPS sample originated from the 460 nm scintillation ($^1G_4 \rightarrow {}^3H_6$ transition). These slow components are similar to the calculated decay time constant of the Tm^{3+} $^1G_4 \rightarrow {}^3H_6$ transition in Tm-doped $KLa(WO_4)_2$ (KLWO).[36]

Figure 7 shows the afterglow timing profiles of the Tm-doped LaPS and LPS samples. Before the afterglow measurement, both samples were annealed at 350 °C for 10 min. Despite the annealing, the Tm-doped LaPS sample still showed a higher background scintillation intensity than the Tm-LPS counterpart. Af_{20} results were 61 and 332 ppm for the Tm-doped LPS and Tm-

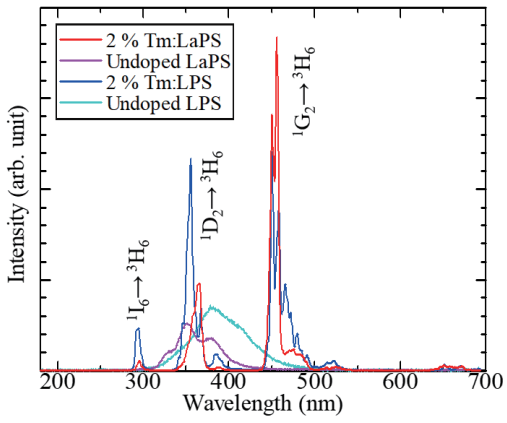

Fig. 5. (Color online) X-ray-induced scintillation spectra of Tm-doped LaPS and LPS samples with undoped LaPS and LPS.

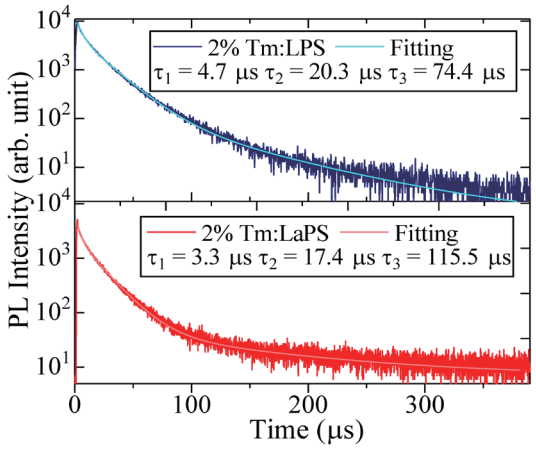

Fig. 6. (Color online) X-ray-induced scintillation decay time profiles of Tm-doped LaPS and LPS samples.

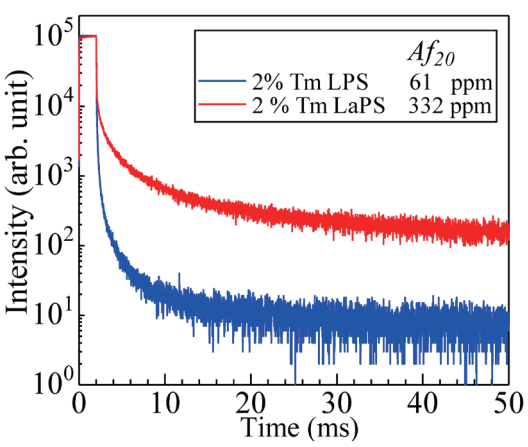

Fig. 7. (Color online) Afterglow timing profiles of Tm-doped LaPS and LPS samples.

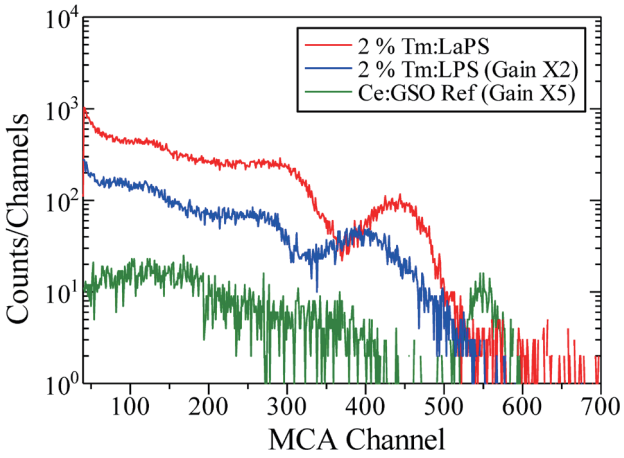

Fig. 8. (Color online) ^{137}Cs γ-ray-irradiated pulse-height spectra of Tm-doped LaPS and LPS samples with Ce-doped GSO reference.

doped LaPS samples, respectively. When compared with the commercially available scintillator, the Tm-doped LPS sample has lower afterglow levels than the conventional inorganic scintillators such as $Bi_4Ge_3O_{12}$ (BGO) at 150 ppm[39] and $CdWO_4$ (CWO) at 100 ppm.[40] On the other hand, the Tm-doped LaPS sample has a slightly higher afterglow level than similar scintillators.

^{137}Cs γ-ray-irradiated (662 keV) pulse-height spectra of the Tm-doped LaPS and LPS samples with the Ce-doped GSO reference are shown in Fig. 8. The Ce-doped GSO reference in this figure has a scintillation light yield of 7000 ph/MeV. The scintillation light yield in this measurement was calculated by considering the PMT efficiency in each scintillation wavelength with the ±10% error from the optical attachment and Gaussian fitting. Results showed that 2.0% Tm-doped LPS has a higher scintillation light yield than LaPS at 2340 and 1440 ph/MeV. In addition, when considering the second and third scintillation decay time components of both samples, the maximum shaping time for this measurement setup at 10 μs cannot accommodate all the scintillations of both the Tm-doped LaPS and LPS samples. Therefore, the scintillation light yield in this measurement is underestimated. The pulse-height setup with the longer shaping time (100 μs) can be used to measure the actual scintillation light yields of these two compounds.

4. Conclusions

2.0% Tm-doped LaPS and LPS single crystals were successfully synthesized using a dual-halogen-type desktop floating zone furnace. XRD patterns indicated a single phase for both the LPS and LaPS samples without an impurity phase. Both samples showed similar PL emissions at 450 nm from the Tm^{3+} 4f–4f transition with similar PL *QY* values at around 5.0%. PL decay times were 81.6 and 118.6 μs for the Tm-doped LPS and LaPS samples, respectively. X-ray-

induced scintillation spectra showed three emission peaks from the different ground states of the Tm^{3+} 4f–4f transition. The afterglow levels at 20 ms after X-ray irradiation were 61 ppm for the Tm-doped LPS sample and 332 ppm for the Tm-doped LaPS sample. In pulse height spectra, the 2.0% Tm-doped LPS sample showed a higher scintillation light yield than the LaPS counterpart at 2340 and 1440 ph/MeV. Finally, with the same 2.0% Tm doping, the Tm-doped LPS sample showed more compelling scintillation properties for the scintillation detector scenario than the Tm-doped LaPS sample, including a lower afterglow level and a higher scintillation light yield under 662 keV γ-ray irradiation.

Acknowledgments

This work was supported by the Cooperative Research Project of the Research Center for Biomedical Engineering, Iketani Science and Technology, Nippon Sheet Glass Foundation, NAIST special fund, and Japan Society for the Promotion of Science (JSPS) under Grants-in-Aid for Early-Career Scientists (20K20104) and Scientific Research B (19H03533, 21H03733, and 21H03736).

References

1 M. Kole, M. Chauvin, Y. Fukazawa, K. Fukuda, S. Ishizu, M. Jackson, T. Kamae, N. Kawaguchi, T. Kawano, M. Kiss, E. Moretti, M. Pearce, S. Rydström, H. Takahashi, and T. Yanagida: Nucl. Instrum. Methods Phys. Res., Sect. A **770** (2015) 68.
2 A. Khan, P. Q. Vuong, G. Rooh, H. J. Kim, and S. Kim: J. Alloys Compd. **827** (2020) 154366.
3 C. L. Melcher: Nucl. Instrum. Methods Phys. Res., Sect. B **40–41** (1989) 1214.
4 J. Glodo, Y. Wang, R. Shawgo, C. Brecher, R. H. Hawrami, J. Tower, and K. S. Shah: Phys. Procedia **90** (2017) 285.
5 M. Koshimizu, T. Yanagida, R. Kamishima, Y. Fujimoto, and K. Asai: Sens. Mater. **31** (2019) 1233.
6 D. Shiratori, D. Nakauchi, T. Kato, N. Kawaguchi, and T. Yanagida: Sens. Mater. **32** (2020) 1365.
7 N. Kawaguchi, H. Masai, M. Akatsuka, D. Nakauchi, T. Kato, and T. Yanagida: Sens. Mater. **33** (2021) 2215.
8 N. Kawaguchi and T. Yanagida: Sens. Mater. **31** (2019) 1257.
9 F. Zaman, N. Srisittipokakun, G. Rooh, J. Kaewkhao, I. Ullah, M. Rani, and H. J. Kim: J. Non-Cryst. Solids **561** (2021) 120722.
10 D. Shiratori, D. Nakauchi, T. Kato, N. Kawaguchi, and T. Yanagida: Sens. Mater. **32** (2020) 1365.
11 H. Fukushima, M. Akatsuka, H. Kimura, D. Onoda, D. Shiratori, D. Nakauchi, T. Kato, N. Kawaguchi, and T. Yanagida: Sens. Mater. **33** (2021) 2235.
12 M. Akatsuka, H. Kimura, D. Onoda, D. Shiratori, D. Nakauchi, T. Kato, N. Kawaguchi, and T. Yanagida: Sens. Mater. **33** (2021) 2243.
13 G. Okada, M. Akatsuka, H. Kimura, M. Mori, N. Kawano, N. Kawaguchi, and T. Yanagida: Sens. Mater. **30** (2018) 1547.
14 D. Nakauchi, N. Kawaguchi, and T. Yanagida: Sens. Mater. **31** (2019) 1249.
15 K. Sreebunpeng, P. Janthon, W. Chewpraditkul, T. Szczesniak, M. Nikl, and A. Yoshikawa: Opt. Mater. **108** (2020) 110161.
16 D. Nakauchi, T. Kato, N. Kawaguchi, and T. Yanagida: Sens. Mater. **32** (2020) 1389.
17 H. Kimura, T. Kato, D. Nakauchi, M. Koshimizu, N. Kawaguchi, and T. Yanagida: Sens. Mater. **31** (2019) 1265.
18 D. Shiratori, T. Kato, D. Nakauchi, N. Kawaguchi, and T. Yanagida: Sens. Mater. **33** (2021) 2171.
19 H. Kimura, T. Kato, D. Nakauchi, N. Kawaguchi, and T. Yanagida: Sens. Mater. **32** (2020) 1381.
20 D. Nakauchi, T. Kato, N. Kawaguchi, and T. Yanagida: Sens. Mater. **32** (2020) 1389.
21 A. Horimoto, N. Kawano, D. Nakauchi, H. Kimura, M. Akatsuka, and T. Yanagida: Sens. Mater. **32** (2020) 1395.
22 M. Koshimizu, N. Kawano, A. Kimura, S. Kurashima, M. Taguchi, Y. Fujimoto, and K. Asai: Sens. Mater. **33** (2021) 2137.

23 L. Pidol, A. Khan-Harari, B. Viana, B. Ferrand, P. Dorenbos, J. T. M. De Haas, C. W. E. Van Eijk, and E. Virey: J. Phys. Condens. Matter **15** (2003) 2091.
24 P. Kantuptim, H. Fukushima, H. Kimura, D. Nakauchi, T. Kato, M. Koshimizu, N. Kawaguchi, and T. Yanagida: Sens. Mater. **33** (2021) 2195.
25 T. Yanagida, K. Watanabe, G. Okada, and N. Kawaguchi: Jpn. J. Appl. Phys. **57** (2018) 106401.
26 P. Kantuptim, T. Kato, D. Nakauchi, N. Kawaguchi, and T. Yanagida: Jpn. J. Appl. Phys. **61** (2022) SB1038.
27 Q. Wei, G. Liu, Z. Zhou, J. Wan, H. Yang, and Q. Liu: Mater. Lett. **126** (2014) 178.
28 P. Kantuptim, M. Akatsuka, D. Nakauchi, T. Kato, N. Kawaguchi, and T. Yanagida: J. Alloys Compd. **847** (2020) 156542.
29 T. Yanagida, K. Kamada, Y. Fujimoto, H. Yagi, and T. Yanagitani: Opt. Mater. **35** (2013) 2480.
30 T. Yanagida, Y. Fujimoto, T. Ito, K. Uchiyama, and K. Mori: Appl. Phys. Express **7** (2014) 18.
31 T. Yanagida, N. Kawaguchi, Y. Fujimoto, K. Fukuda, K. Watanabe, A. Yamazaki, and A. Uritani: J. Lumin. **144** (2013) 212.
32 I. A. Bondar: Ceram. Int. **8** (1982) 83.
33 X. Ye, Y. Luo, S. Liu, D. Wu, D. Hou, and F. Yang: J. Rare Earths **35** (2017) 927.
34 M. Sugiyama, Y. Fujimoto, T. Yanagida, D. Totsuka, Y. Yokota, and A. Yoshikawa: Opt. Mater. **34** (2011) 439.
35 G. Jia, C. Tu, Z. You, J. Li, Z. Zhu, and B. Wu: Solid State Commun. **134** (2005) 583.
36 L. Macalik, J. Hanuza, D. Jaque, and J. García Solé: Opt. Mater. **28** (2006) 980.
37 T. Yanagida, N. Kawaguchi, K. Fukuda, S. Kurosawa, Y. Fujimoto, Y. Futami, Y. Yokota, K. Taniue, H. Sekiya, H. Kubo, A. Yoshikawa, and T. Tanimori: Nucl. Instrum. Methods Phys. Res., Sect. A **659** (2011) 258.
38 Y. Fujimoto, M. Sugiyama, T. Yanagida, S. Wakahara, S. Suzuki, S. Kurosawa, V. Chani, and A. Yoshikawa: Opt. Mater. **35** (2013) 2023.
39 Saint Gobain Crystal: BGO Bismuth Germanate Scintillation Material (2016).
40 L. Nagornaya, G. Onyshchenko, E. Pirogov, N. Starzhinskiy, I. Tupitsyna, V. Ryzhikov, Y. Galich, Y. Vostretsov, S. Galkin, and E. Voronkin: Nucl. Instrum. Methods Phys. Res., Sect. A **537** (2005) 163.